Nanoscale Res Lett (2008) 3:169–178
DOI 10.1007/s11671-008-9132-6

NANO EXPRESS

Fabrication and Properties of Porphyrin Nano- and Micro-particles with Novel Morphology

Xiangqing Li · Line Zhang · Jin Mu · Jinlong Qiu

Received: 28 October 2007 / Accepted: 5 May 2008 / Published online: 21 May 2008

Abstract New types of porphyrin nano- and micro-particles composed of J- and H-heteroaggregates were prepared by electrostatic self-assembly of two oppositely charged porphyrins, tetrakis(4-trimethylammoniophenyl)porphyrin (H_2TAPP^{4+}) and tetrakis(4-sulfonatophenyl)porphyrin cobalt (II) ($CoTPPS^{4-}$), in aqueous solutions. Transmission electron microscopy (TEM) images showed novel morphology and size distribution of porphyrin particles fabricated under different experimental conditions. The assembly process of the nano- and micro-particles was monitored by UV–Vis spectra. Fluorescence spectra and UV–Vis spectra provided optical information on the formation of the nano- and micro-particles. Cyclic voltammograms of the porphyrin particles indicated that the electron gain and loss of the H_2TAPP^{4+} ion were restrained, and the electron transfer of the $CoTPPS^{4-}$ ion was promoted in the J- and H-type porphyrin heteroaggregates within the particles. The stability and constitution of the nano- and micro-particles were confirmed by UV-light irradiation, heat-treatment, and pH and ionic strength changes. Photoelectrochemical measurements showed that the photoelectron transfer of TiO_2 modified with the particles was more efficient than that of TiO_2 sensitized by either monomers. The photoelectronic and photocatalytic properties of the products indicated that the pyramidal or spherical configuration of the nano- and micro-particles was favorable for the absorption and transfer of the energy. It can be found that TiO_2 sensitized by the porphyrin nano- and micro-particles exhibits significant improvement in energy conversion and photocatalytic activity with reference to pure TiO_2.

Keywords Porphyrins · Self-assembly · Heteroaggregates · Morphology · Properties

X. Li · L. Zhang · J. Mu (✉) · J. Qiu
Department of Chemistry, Key Laboratory for Ultrafine Materials of Ministry of Education, East China University of Science and Technology, P.O. Box 427, 130 Meilong Road, Shanghai 200237, China
e-mail: jinmu@ecust.edu.cn

Introduction

Functionalized self-assembled materials with well-defined shapes and dimensions are of wide applications in electronics, photonics, light energy conversion, and catalysis [1, 2]. The possibility of changing mesoscopic structures of the resulting species through a proper choice of the molecular components opens a way to design and synthesize materials capable of exhibiting specific properties and functions.

Porphyrins and other tetrapyrroles are attractive building blocks for functional nanostructures. With the appropriate selection of substituents, noncovalent self-assembly can occur via intermolecular electrostatic interaction, hydrogen bonding, and metal coordination. In recent years, a variety of nanoscale self-assembled structures using porphyrins have been reported [3, 4]. Fuhrhop and co-workers [5] have demonstrated that amphiphilic porphyrins aggregate in an aqueous solution in the form of fibers, ribbons, and tubules. Hydrogen bonding, van der Waals interactions, and hydrophobic effects are the major driving forces to achieve such ordered assemblies of these molecules. A diacid form of meso-tetrakis(4-sulfonatophenyl)porphyrin at very low pH, or in the presence of various inorganic and organic cations, is able to form J-aggregates in which the zwitterionic porphyrins are arranged in a side-by-side stacking structure [6–9]. A dicationic porphyrin (*trans*-bis(4-N-methylpyridinium)diphenylporphine) aggregates, forming large, rigid, and almost monodispersed clusters, with a fractal structure [10], in which the aggregation

is controlled by salt concentration, or by screening the charge repulsion by changes in the ionic strength, pH, etc. The architectures of meso-/nano-scale porphyrin assemblies or particles are expected to be promising candidates for use in photonic devices [11, 12]. Several mimetic systems of porphyrin aggregates have been designed and exploited as light harvesting systems for artificial photosynthetic systems and for molecular devices [13]. The structural, kinetic, and spectroscopic studies on porphyrin J- and H-aggregates can provide useful information for understanding intermolecular interaction in the aggregation processes and for applications of these materials in molecular devices.

Sensitization of wide band-gap semiconductor electrodes with organic dye molecules has been a field of extensive research over past decades due to the potential application in solar energy conversion [14]. The organic dyes deposited on a semiconductor electrode surface are used to absorb incident light. The light absorption of the dye is followed by an electron injection from the excited state of the dye into the conduction band of the semiconductor. Efforts have been made in the past to employ porphyrin derivatives to sensitize TiO_2 electrodes [15–17], for porphyrin compounds possess good chromophore activities over the solar spectrum and good electron donating properties due to their large π-electron systems, which lead to facile ionization. The favorable energy of charge transfer states and also their lifetimes are advantageous in prompting the utilization of porphyrin complexes as light harvesting donor molecules in donor–acceptor assemblies [18]. It is reported that H- or J-type aggregates of porphyrins play a role as light harvesting assemblies to gather and transfer energy to the assembled devices, and to obtain a higher incident photon-to-photocurrent generation efficiency [19–21]. A great deal of studies have highlighted the performance of TiO_2 used as environmental photocatalysts to remove some organic compounds, such as dyes [22–25]. Nevertheless, there are few reports about porphyrin nano- and micro-particles made up of J- and H-heteroaggregates to date [26]. The photocatalytic and photoelectronic properties of TiO_2 sensitized with this type of porphyrin nano- and micro-particles have not been studied. Therefore, an exploration of the porphyrin nano- and micro-particles is critical and necessary.

Considering that the structure of porphyrin aggregates is strongly dependent on the experimental conditions [27], it is worthwhile to extend this investigation to other porphyrin aggregates. Furthermore, it is interesting to modulate the mesoscopic structure of the aggregates by imposing chemical changes to the monomer. Water-soluble porphyrins are suitable for building blocks because, depending on their electronic and steric properties, they can self-assemble spontaneously into dimers or higher aggregates via noncovalent interactions.

In the present work, the porphyrin nano- and microparticles, composed of J- and H-type porphyrin heteroaggregates of tetrakis(4-sulfonatophenyl)porphyrin cobalt ($CoTPPS^{4-}$) and tetrakis(4-trimethylammoniophenyl)porphyrin (H_2TAPP^{4+}) (Scheme 1), were prepared in various experimental conditions by an "ion-association technique"

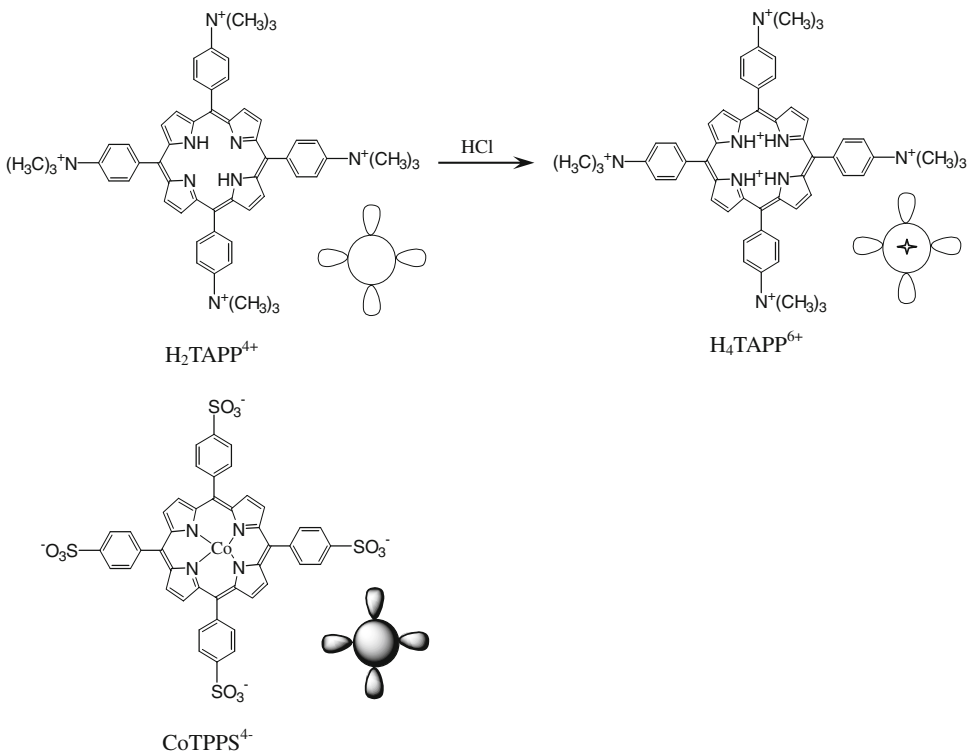

H_2TAPP^{4+} H_4TAPP^{6+}

$CoTPPS^{4-}$

Scheme 1 Structures and models of H_2TAPP^{4+}, H_4TAPP^{6+}, and $CoTPPS^{4-}$

that has advantages in simplicity and versatility [28]. The selection of two porphyrin monomers is dependent on the six positive charges in the center and the peripheries of a H_4TAPP^{6+} ion (obtained by acidification of a H_2TAPP^{4+} ion) and four negative charges in the peripheries of a $CoTPPS^{4-}$ ion, which make it possible to drive the formation of J- and H-type porphyrin heteroaggregates in the *xy* plane and along the *z* direction by coulombic attraction, respectively. The interaction between the H_4TAPP^{6+} ion and the $CoTPPS^{4-}$ ion in aqueous solution are characterized with UV–Vis spectra and fluorescence spectra. The images of TEM and the results of UV–Vis and fluorescence spectra show that the porphyrin nano- and micro-particles are successfully synthesized. The stability, electrochemical, photoelectrochemical, and photocatalytic activities of the porphyrin nano- and micro-particles are also investigated in detail.

Experimental Details

Materials

Tetrakis(4-trimethylammoniophenyl)porphyrin iodide (H_2TAPP^{4+}) was prepared in *N*,*N*-dimethylformamide with tetrakis(4-trimethylammoniophenyl)porphyrin (H_2TAPP) and iodomethane as reactants and purified similar to the method reported elsewhere [5, 11]. The H_2TAPP was obtained by refluxing p-dimethylaminobenzaldehyde and pyrrole in n-butanoic acid for 30 min. Tetrakis(4-sulfonatophenyl)porphyrin cobalt ($CoTPPS^{4-}$) was prepared by using the method previously described by Adler et al. [29]. TiO_2 powder was prepared from the hydrolysis of titanium isopropoxide [30]. All the other reagents and solvents were obtained from commercial sources and used without further purification.

Preparation of Porphyrin Nano- and Micro-particles

The porphyrin nano- and micro-particles comprised of J- and H-porphyrin heteroaggregates were formed by mixing aqueous solutions of the two porphyrins shown in Scheme 1. Typically, the H_2TAPP^{4+} solution (20 mL, 21 μmol L^{-1}) was acidulated with hydrochloric acid (20 mL, 2 mol L^{-1}). The color of the solution was immediately changed from light purple to green due to the protonation of the H_2TAPP^{4+} ion to form the H_4TAPP^{6+} monomer, then the $CoTPPS^{4-}$ solution (20 mL, 7 μmol L^{-1}) was added into the H_4TAPP^{6+} solution. The mixture was placed in the dark for 72 h. The other porphyrin nano- and micro-particles in various proportions of the reagents (shown in Table 1) were prepared to investigate the formation process, morphology, and size control of the porphyrin nano- and micro-particles.

Electrochemical Experiments

The cyclic voltammograms were obtained on a PCI 4/300 electrochemical analyzer (GAMRY Instruments, USA) in a standard three-electrode cell consisting of a glass carbon electrode (GCE) as the working electrode, a platinum electrode as the counter electrode, and an Ag/AgCl electrode as the reference electrode. After bubbling N_2 into the system for 30 min, cyclic voltammetric experiments were performed at a scan rate of 80 mV s^{-1} in the supporting electrolyte solution of $NaClO_4$ (1.0 mol L^{-1}).

Photoelectrochemical Measurements

Photoelectrochemical measurements were performed in an assembled cell consisting of a working electrode (FTO/TiO_2/porphyrins, FTO is the fluoride-doped tin oxide electrode) and a counter electrode (Pt/FTO), as shown in Scheme 2. Nanostructured TiO_2 films were cast on an FTO substrate from a colloidal solution prepared from the hydrolysis of titanium isopropoxide [31], and then the electrode was treated by dipping it into the porphyrin monomers or the particles solution for 24 h. The electrode was washed with distilled deionized water. The color of the electrode changed from white to purple for $CoTPPS^{4-}$ and to green for H_4TAPP^{6+} and porphyrin particles, indicating that the porphyrins were coated on the electrode. All photoelectrochemical measurements were carried out in acetonitrile containing 0.5 mol L^{-1} LiI and 0.01 mol L^{-1} I_2 as supporting electrolytes on a Keithley model 617 programmable electrometer (USA). A collimated

Table 1 Dosage of reagents for various porphyrin nano- and micro-particles

	H_2TAPP^{4+}	$CoTPPS^{4-}$	H_2TAPP^{4+}:$CoTPPS^{4-}$ (molar ratio)	HCl
Sample 1	20 mL	20 mL	3:1	20 mL
	21 μmol L^{-1}	7 μmol L^{-1}		2 mol L^{-1}
Sample 2	20 mL	20 mL	1:3	20 mL
	7 μmol L^{-1}	21 μmol L^{-1}		2 mol L^{-1}
Sample 3	20 mL	20 mL	1:3	20 mL
	7 μmol L^{-1}	21 μmol L^{-1}		0.04 mol L^{-1}
Sample 4	20 mL	20 mL	1:9	0
	1 μmol L^{-1}	9 μmol L^{-1}		

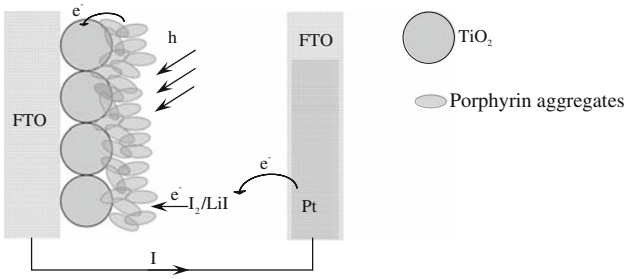

Scheme 2 Scheme of the assembled cell for photoelectrochemical measurements

light beam from a 150 W Xenon lamp with a 370 nm cut-off filter was used for excitation of the porphyrins film cast on the TiO_2 electrode.

Photocatalysis Measurements

The photocatalytic degradation of Rhodamine B was carried out at 28 °C in a quartz calorimetric vessel of 50 mL by irradiation from a 300 W high pressure mercury lamp. The solution consisted of 0.02 g photocatalyst (TiO_2, or TiO_2/porphyrin composites in which the porphyrin was $CoTPPS^{4-}$, or H_4TAPP^{6+}, or porphyrin nano- and micro-particles), and Rhodamine B (20 mL, 1×10^{-4} mol L^{-1}). The TiO_2/porphyrin composites were prepared by stirring TiO_2 (0.02 g) with the following solutions: (a) H_2TAPP^{4+} (20 mL, 3.5×10^{-5} mol L^{-1}) and HCl (10 mL, 2 mol L^{-1}); (b) $CoTPPS^{4-}$ (20 mL, 1×10^{-4} mol L^{-1}) and HCl (10 mL, 2 mol L^{-1}); (c) porphyrin nano- and micro-particles assembled by mixing the solutions of $CoTPPS^{4-}$ (20 mL, 1×10^{-4} mol L^{-1}), H_2TAPP^{4+} (20 mL, 3.5×10^{-5} mol L^{-1}) and HCl (20 mL, 2 mol L^{-1}), respectively. The distance between the UV-lamp and the sample was kept 10 cm. The absorbance of the solution was recorded at certain time intervals.

Other Characterization

The UV–Vis spectra were measured on a UV-2102 UV–Vis spectrophotometer (Unico, China). The fluorescence spectra were recorded with a RF-5301PC spectrophotometer (Shimadzu, Japan). The TEM images were collected on a JEOL JEM-1200 EX11 transmission electron microscopy (Japan). The SEM images were achieved on a JEOL JSM-6360 LV scanning electron microscopy (Japan).

Results and Discussion

TEM Images of the Porphyrin Nano- and Micro-particles

The TEM images of sample 1 are shown in Fig. 1a, b. Two types of porphyrin particles with different shapes are found. The length of the sides of these pyramids in Fig. 1a is in the range of 160–260 nm. The porphyrin microspheres are uniform, with an average diameter of approximately 900 nm (Fig. 1b). Interestingly, the pyramids are inhomogeneous but translucent or alternating with light and shade. It is probably due to the different response of the metalloporphyrin ($CoTPPS^{4-}$) and non-metalloporphyrin (H_4TAPP^{6+}) in the pyramidal particles to the bombardment of electron beams, which is one of the proofs that the pyramids consist of $CoTPPS^{4-}$ and H_4TAPP^{6+}.

Figure 1c, d shows the images of samples 2 and 3, respectively. In Fig. 1c, the diameter of the spheres is in the range of 250–1,300 nm, which has a larger distribution than the spheres formed in sample 1. In Fig. 1d, the diameter of the porphyrin nanoparticles distributes in the range of 80–120 nm, which is much smaller than that of sample 2.

The morphology of sample 4 assembled by the electrostatic interaction of the periphery substituents of the H_2TAPP^{4+} and $CoTPPS^{4-}$ ions shows irregular microspheres in which contain many porphyrin J- and H-heteroaggregates with the diameter of about 60–150 nm (Fig. 1e).

As can be seen in Scheme 1, the peripheries and the center of a H_4TAPP^{6+} ion supply six positive charges, and the peripheries of a $CoTPPS^{4-}$ ion give four negative charges. So the periphery substituents with opposite charges can be linked to each other by electrostatic interaction in the *xy* plane. Besides, a H_4TAPP^{6+} ion can supply another two positive charges located at the center. Because of the interactions among the central two positive charges of a H_4TAPP^{6+} ion and the periphery negative charges of a $CoTPPS^{4-}$ ion, the J-aggregates in the *xy* plane can be further linked by the $CoTPPS^{4-}$ ion along the *z* direction to form larger J- and H-heteroaggregates. The porphyrin nano- and micro-particles are obtained by static interaction of many J- and H-heteroaggregates.

Based on the experiments, there are two main factors that could influence the shape and the size distribution of the porphyrin particles. For one thing, it is the molar ratios of two kinds of porphyrin in the solution. The structures of two porphyrins (Scheme 1) and the formation mechanism of the sphere-like particles (see Ref. 26) show that a $[H_4TAPP]^{6+}$ ion supplies more charges than a $[CoTPPS]^{4-}$ ion, so more $[CoTPPS]^{4-}$ ions are needed in the formation of the sphere-like particles. In sample 2, the sphere-like particles are obtained (the molar ratio of $[H_4TAPP]^{6+}$ to $[CoTPPS]^{4-}$ is 1:3). With the reaction prolonging, the concentration of the porphyrin monomers decreases. As a result, the smaller sphere-like particles are formed in the solution. So a larger size distribution can be observed in Fig. 1c. When the $[CoTPPS]^{4-}$ is relatively inadequate in the solution, for example, in sample 1 (the molar ratio of

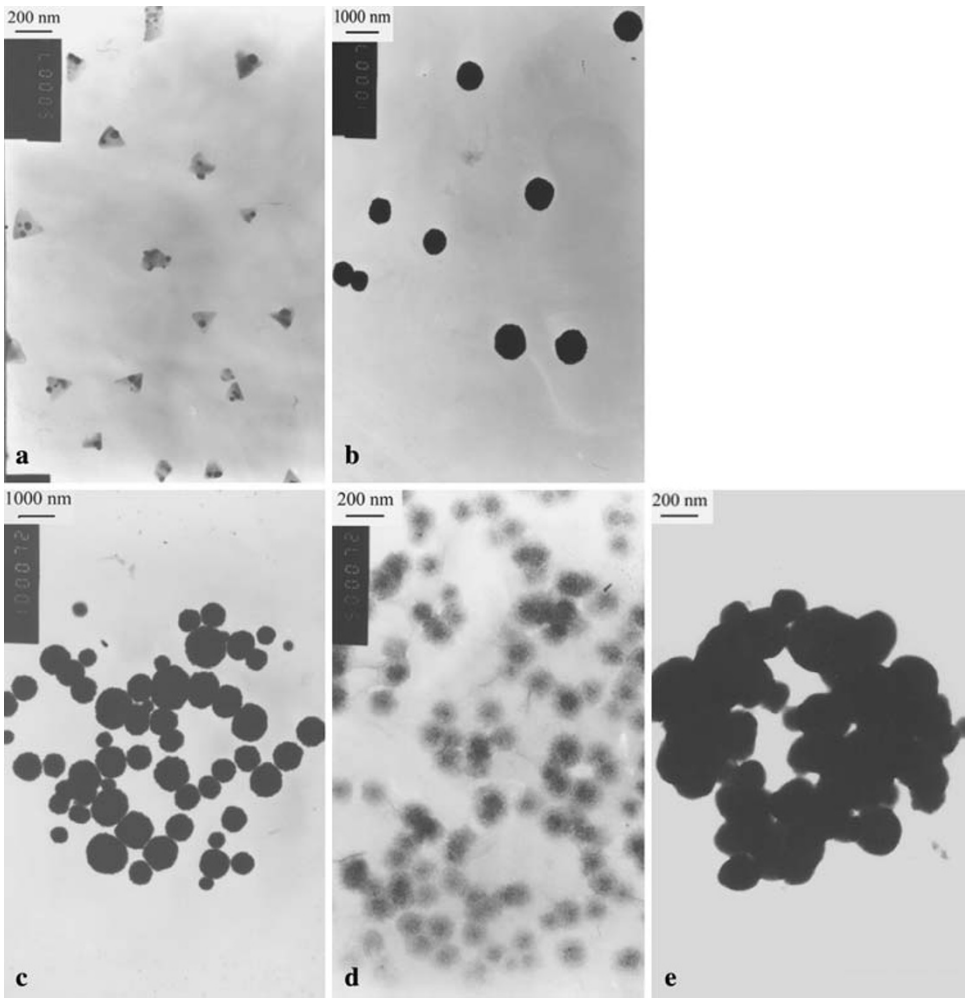

Fig. 1 TEM images of sample 1 (**a**–**b**), sample 2 (**c**), sample 3 (**d**), and sample 4 (**e**)

$[H_4TAPP]^{6+}$ to $[CoTPPS]^{4-}$ is 3:1), the pyramid-like particles in which fewer amounts of $[CoTPPS]^{4-}$ is needed are easy to be produced. Along with the proceeding of the reaction, the ratio of $[H_4TAPP]^{6+}$ to $[CoTPPS]^{4-}$ decreases, namely, the relative content of $[CoTPPS]^{4-}$ increases, which is favorable to the formation of the sphere-like particles. Therefore, both pyramid-like and sphere-like particles can be observed in sample 1. As a result, when the $[CoTPPS]^{4-}$ in the solution is adequate, the porphyrin monomers prefer forming the sphere-like particles and, when the $[CoTPPS]^{4-}$ is inadequate, forming the pyramid-like and sphere-like particles.

For another, the acidity of the solution affects the size of the particles. The complete protonation of two nitrogen atoms in the center of the $[H_2TAPP]^{4+}$ ion can promote the growth of the H-aggregates in the *z* direction, and the larger particles (samples 1 and 2) are formed. The poor protonation in the center of $[H_2TAPP]^{4+}$ will restrain the growth of the H-aggregates along the *z* direction. So the smaller particles are formed in sample 3.

The formation mechanism of sample 4 is shown in Scheme 3. In the *xy* plane, the J-aggregates of the

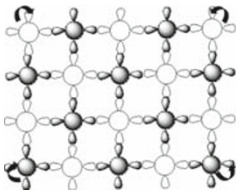

, and represent $[H_2TAPP]^{4+}$, and $[CoTPPS]^{4}$, respectively.

Scheme 3 The formation mechanism of sample 4

$[H_2TAPP]^{4+}$ and $[CoTPPS]^{4-}$ are assembled by the electrostatic interaction of the periphery substituents of two porphyrins. As shown by the arrows in Scheme 3, the J-aggregates can bend to form irregular spheres by the action of gravity.

UV–Vis Spectra

The formation process of sample 4 is monitored by UV–Vis spectra. As shown in Fig. 2A, the Soret band of the as-mixed solution is at 412 nm [see Fig. 2A(a)]. Along with the reaction, the Soret band at 412 nm gradually decreases;

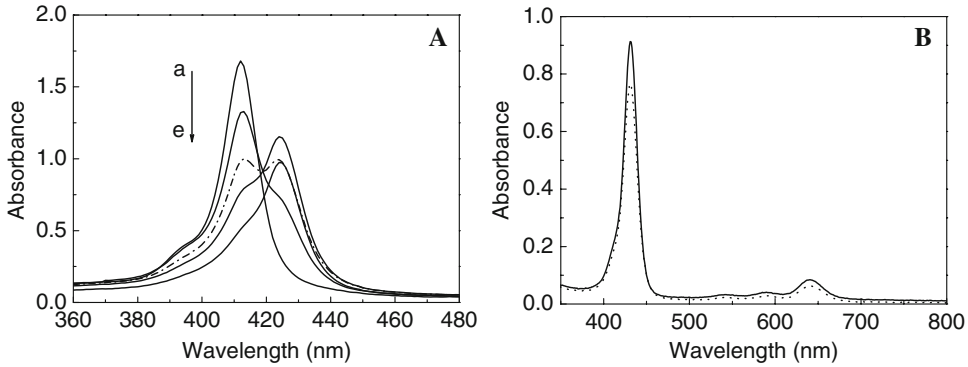

Fig. 2 (**A**) UV–Vis spectra of the formation process of sample 4, as-mixed (a), placed for 24 h (b), 48 h (c, dot line), 56 h (d), and 72 h (e); (**B**) UV–Vis spectra of sample 2 solution, as-mixed (dotted line) and placed for 72 h (solid line)

when placed for 48 h, the band at 412 nm splits, and new broad bands at 412 and 424 nm with the same intensity are observed. After standing for 72 h, the band at 412 nm almost disappears.

The porphyrin heteroaggregation in samples can be deduced from the changes of the porphyrin Soret absorption bands. The shape and location of the Soret band are extremely sensitive to the changes in microenvironment of the porphyrin moiety [32]. The occurrence of the new band at 424 nm and intensity decreasing of the Soret band imply the aggregation of the free porphyrins. The band at 424 nm can be classified as a J-aggregate. The red-shift of the spectrum can be attributed to the excitonic coupling between monomer transition dipole of $CoTPPS^{4-}$ and that of H_2TAPP^{4+} in the formation process of porphyrin nano- and micro-particles [33, 34].

The Soret and Q bands of sample 2 solution placed for 72 h are not shifted, and the absorption intensity increases, in comparison to those of the as-mixed solution. The UV–Vis spectra of samples 1 and 3 (as-mixed and placed for 72 h) are similar to that of sample 2. It is probably due to the simultaneous formation of both H- and J-heteroaggregates in porphyrin nano- and micro-particles [33, 35–37].

The UV–Vis spectra of two kinds of porphyrins ($CoTPPS^{4-}$ and H_2TAPP^{4+}) (not shown here) demonstrated that the $CoTPPS^{4-}$ ions are stable in the 2 mol L^{-1} hydrochloric acid. However, the Soret band of H_2TAPP^{4+} treated with hydrochloric acid (2 mol L^{-1}) is red-shifted and the number of the Q bands reduces, indicating that the two nitrogen atoms in the center of H_2TAPP^{4+} are protonated. The protonated H_2TAPP^{4+} ion (denoted as H_4TAPP^{6+}) can supply another two positive charges in the center, which makes it possible for H_4TAPP^{6+} and $CoTPPS^{4-}$ to form porphyrin particles not only in the horizontal direction but also in the perpendicular direction by static interaction.

Fluorescence Spectra

To confirm the heteroaggregation of porphyrin moieties within the nano- and micro-particles, fluorescence measurements were carried out. The fluorescence spectra (as-mixed and placed for 24 h) of sample 4 show a new emission band at 601 nm. Furthermore, the intensity of the intrinsic emission bands (at 646 and 700 nm) for H_2TAPP^{4+} decreases along with the process of reaction, and the position moves to 647 and 705 nm, respectively. The fluorescence spectrum of sample 4 exhibits the bathochromic shift in comparison to that of the as-mixed solution, corresponding to the behavior observed in the UV–Vis spectra.

The red shifts in fluorescence peaks of sample 4 are due to increased resonance interaction between the two porphyrin monomers ($CoTPPS^{4-}$ and H_2TAPP^{4+}) in the singlet excited state. Compared to the as-mixed solution of two porphyrin monomers, the decreased quantum yield of sample 4 is attributed to the heavy sulfur atoms and Co ions in the porphyrin particles [38]. The changed spectrum indicates that a new compound is formed in the solution and the J-heteroaggregates are present in the particles.

However, the emission bands of sample 2 are not moved and the emission intensity of the solution increases after placed for 72 h, which is also similar to that of the UV–Vis spectra. The fluorescence spectra of samples 1 and 3 (as-mixed and placed for 72 h) are same as that of sample 2 (Fig. 3)

Cyclic Voltammetry Studies

Electrochemical studies were performed to evaluate the electronic properties of $CoTPPS^{4-}$, H_4TAPP^{6+}, and sample 2. As can be seen in Fig. 4a, the $CoTPPS^{4-}$ shows two reduction peaks at −0.051 and −0.388 V, respectively, and an oxidation peak at +0.446 V. The peaks originate from the oxidation-reduction reaction between $Co(II)TPPS^{4-}$ and $Co(III)TPPS^{4-}$ in the solution [39]. In Fig. 4b, the H_4TAPP^{6+} displays a redox couple at +0.576 and +0.454 V, respectively, which can be ascribed to the gain and loss of protons bonded with the nitrogen atoms in the center of the H_4TAPP^{6+} [40]. The cyclic voltammogram of sample 2 (in Fig. 4c) shows two reduction peaks and two oxidation peaks. The reduction peaks are observed at

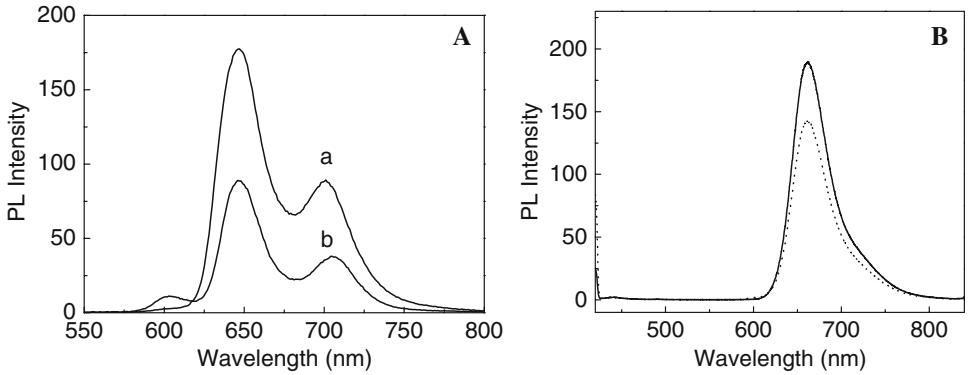

Fig. 3 (**A**) Fluorescence spectra of sample 4 solution, as-mixed (a) and placed for 24 h (b); (**B**) fluorescence spectra of sample 2 solution, as-mixed (dotted line) and placed for 72 h (solid line)

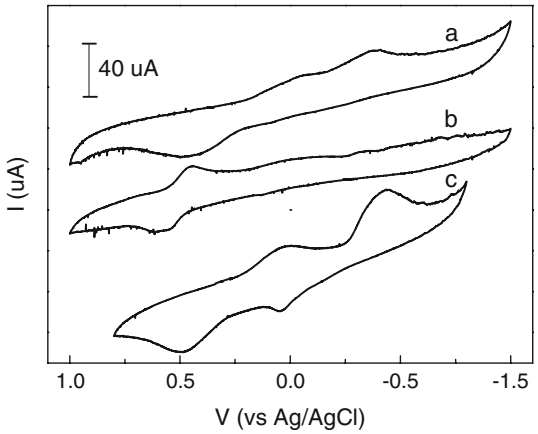

Fig. 4 Cyclic voltammograms of $CoTPPS^{4-}$ (a), H_4TAPP^{6+} (b), and sample 2 (c). The concentrations of $CoTPPS^{4-}$ and H_2TAPP^{4+} in the solutions are shown in Table 1

+0.022 and −0.437 V, and the two oxidation peaks at +0.047 and +0.490 V, respectively. Compared to Fig. 4a, b, it can be observed that the potentials in Fig. 4c increase about 50–70 mV; the oxidation peaks in the center of the H_4TAPP^{6+} cannot be detected; and a new oxidation peak at +0.047 V occurs. It is attributed to the interaction between H_4TAPP^{6+} and $CoTPPS^{4-}$ in the porphyrin nano- and micro-particles, which restrains the gain and loss of protons of the nitrogen atoms bonded with the center of the H_4TAPP^{6+}, and promotes the electron transfer between $Co(II)TPPS^{4-}$ and $Co(III)TPPS^{4-}$.

Stability of Porphyrin Particles

The stability of the porphyrin nano- and micro-particles was examined in different conditions. As can be seen in Fig. 5a, adjusting the ionic strength of the solution by KNO_3 (controlling the concentration of KNO_3 in the solution is 0.1 mol L^{-1}), the morphology of the particles is hardly influenced, and the nanoparticles with diameter distributing in the range of 60−100 nm are obtained after adding KNO_3 into the solution.

Interestingly, it seems that the spherical nanoparticles are etched from the center or the round of the particles after being neutralized to pH = 5–6 by the addition of 0.1 mol L^{-1} $NH_3 \cdot H_2O$ or 0.1 mol L^{-1} NaOH, as shown in Fig. 5b, c respectively.

As shown by the analysis in TEM, sample 2 is formed by the interaction between the center and the peripheral positive charges of H_4TAPP^{6+} and the peripheral negative charges of $CoTPPS^{4-}$. The solution of NaOH can partly neutralize the positive charge of H_4TAPP^{6+} to form H_2TAPP^{4+}, and acidity of the solution is decreased. The spheres or the etched spheres with smaller diameters are obtained (approximatly 60 nm) in Fig. 5c.

For $NH_3 \cdot H_2O$, it can not only neutralize the acid solution, but also interact with the $CoTPPS^{4-}$ by the axial coordination of NH_3 and Co ion in the particles. The image of sample 2 solution treated by 0.1 mol L^{-1} $NH_3 \cdot H_2O$ is the hollow spheres in Fig. 5b, which may be the reason that there are more $CoTPPS^{4-}$ than H_4TAPP^{6+} in the center of particles.

The ultraviolet light irradiation has an influence on the morphology and diameter of sample 2 (Fig. 5d). The spherical particles change into ellipses, and the diameter of the particles distributes in the range of 100–120 nm. As indicated in Fig. 5e, the particles are linked further, and the larger irregular microspheres (about 1 μm) are formed after heat-treatment. The reason is that the J-aggregate is stable in thermodynamics, while the H-aggregate is stable in dynamics, so increasing of temperature promotes the further formation of the J-aggregate in the particles.

It is known that an ultrasonic bath can supply an instantaneous higher temperature (5,000 K) in the microcosmic surroundings [41], which promotes the gather of the particles. As a result, the larger spheres (about 500 nm) are obtained (Fig. 5f) in the solution after being treated with ultrasonic.

Photoelectrochemical Properties of the Porphyrins

In order to evaluate the light energy harvest of porphyrin nano- and micro-particles, three photoelectrochemical cells

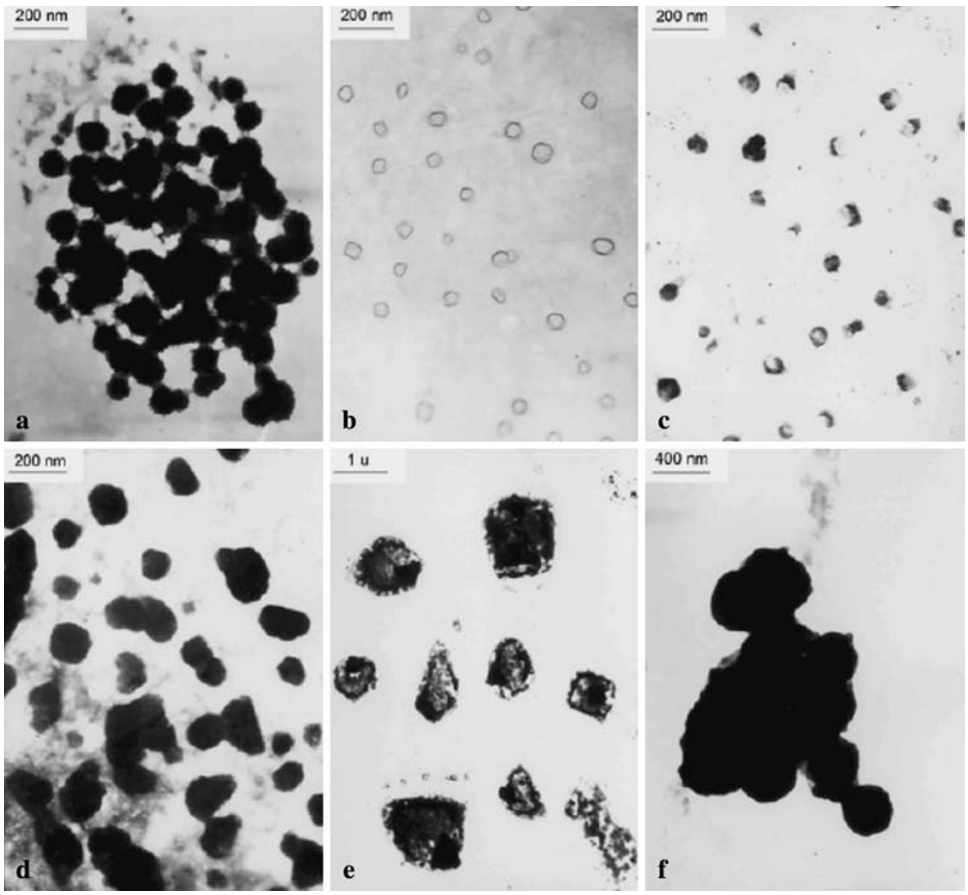

Fig. 5 TEM images of sample 2 solution treated with KNO_3 (**a**), 0.1 mol L^{-1} $NH_3 \cdot H_2O$ (**b**), 0.1 mol L^{-1} NaOH (**c**), UV-light irradiation for 2 h (**d**), heat-treatment at 50 °C for 2 h (**e**), and ultrasonic for 2 h (**f**)

with FTO/TiO_2/porphyrin particles, FTO/TiO_2/H_4TAPP^{6+}, and FTO/TiO_2/$CoTPPS^{4-}$ as the photoanodes are assembled. The I–V characteristics of the three systems are displayed in Fig. 6.

A stable anodic photocurrent generation is observed at applied potential greater than −0.21 V versus SCE. The application of bias positive makes charge separation and charge transport in the FTO/TiO_2/porphyrins electrode more efficient. So the photocurrent increases with increasing bias positive. Potentials could not be scanned beyond +0.3 V since the electrochemical oxidation of iodide will interfere with the photocurrent measurement. In the presence of I_3^-/I^- redox couple, a fairly good stability in the photocurrent is achieved. The redox couple plays a pivotal role in the regenerative nature of the porphyrin-sensitized TiO_2, which is the contribution to charge separation by removing the hole of oxidized porphyrin molecules from the exciton formation region [42]. The oxidized species then diffuse through the electrolyte to the counter electrode.

As expected, the photoelectric conversion ability of the porphyrin particles in the cell is better than the monomers. The porphyrin nano- and micro-particles lead to a larger

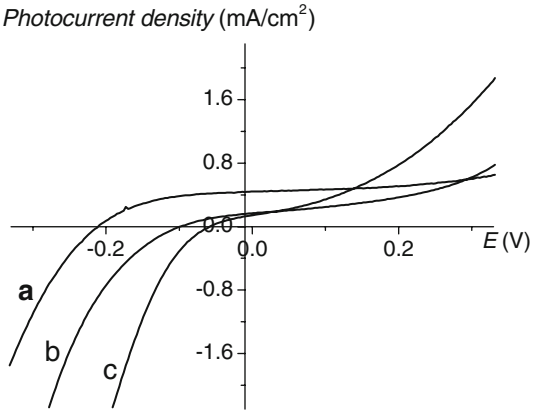

Fig. 6 I–V characteristics of three photoanodes under illumination with white light ($\lambda > 370$ nm): FTO/TiO_2/porphyrin particles (a), FTO/TiO_2/H_4TAPP^{6+} (b), and FTO/TiO_2/$CoTPPS^{4-}$ (c). The solutions corresponding to FTO/TiO_2/porphyrin nano- and micro-particles, FTO/TiO_2/H_4TAPP^{6+}, and FTO/TiO_2/$CoTPPS^{4-}$ electrodes consist of H_2TAPP^{4+} (20 mL, 3.5×10^{-5} mol L^{-1}), $CoTPPS^{4-}$ (20 mL, 1×10^{-4} mol L^{-1}), and HCl (20 mL, 2 mol L^{-1}) (a); H_2TAPP^{4+} (20 mL, 3.5×10^{-5} mol L^{-1}) and HCl (10 mL, 2 mol L^{-1}) (b); $CoTPPS^{4-}$ (20 mL, 1×10^{-4} mol L^{-1}) and HCl (10 mL, 2 mol L^{-1}) (c), respectively. Electrolyte: acetonitrile containing 0.5 mol L^{-1} LiI and 0.01 mol L^{-1} I_2. Input power: 75 mW cm^{-1}

efficiency of photocurrent generation. It is most probably caused by the decreased recombination of photogenerated charges within the porphyrin particles or by an enhanced rate of charge transfer to TiO_2. The observed photocurrent arising from injection of charges from the excited porphyrin molecule to the conduction band of TiO_2 can involve either the singlet or the triplet excited state of the porphyrin [42].

According to the formulas (1) and (2), fill factor (FF) and white light efficiency (η) of the photoanodes are calculated.

$$FF = P_{max}/(V_{oc} \cdot I_{sc}) \quad (1)$$

$$\eta = (FF \cdot V_{oc} \cdot I_{sc})/P_{in} \quad (2)$$

where I_{sc} is short circuit current, V_{oc} is open circuit voltage, P_{in} is input power, and P_{max} is maximal output power. All data are summarized in Table 2.

Photocatalytic Activity of TiO_2/Porphyrin Composites to the Photodegradation of Rhodamine B

As shown in Fig. 7a, the pure TiO_2 is of a lumpy structure, and the surface of TiO_2 is smooth. After being treated with porphyrin solutions, TiO_2 displays the color of the porphyrin, and the surface of TiO_2 contains irregular particles and becomes rough (see Fig. 7b). Accordingly, the porphyrin nano- and micro-particles have been anchored to the smooth surface of the TiO_2.

In order to simulate the dye sensitized semiconductor as a photocatalyst to deal with the contaminated water containing organic dyes, the degradation of Rhodamine B is achieved by TiO_2 sensitized with H_4TAPP^{6+}, $CoTPPS^{4-}$, and the porphyrin nano- and micro-particles, respectively. Plots of absorbance at 553 nm of Rhodamine B versus time are shown in Fig. 8.

Rhodamine B without catalyst is stable under UV-light irradiation, and in the presence of TiO_2/porphyrin composites, the absorbance of Rhodamine B decreases faster than pure TiO_2. It is clearly indicated that the catalytic activity of the porphyrin-sensitized TiO_2 is better. It also can be observed that the photocatalytic activity of the porphyrin particles sensitized TiO_2 is better than the H_4TAPP^{6+}- or $CoTPPS^{4-}$-sensitized one. The difference is ascribed to poor electronic coupling of the two monomers to the titania conduction band, and the pyramidal and

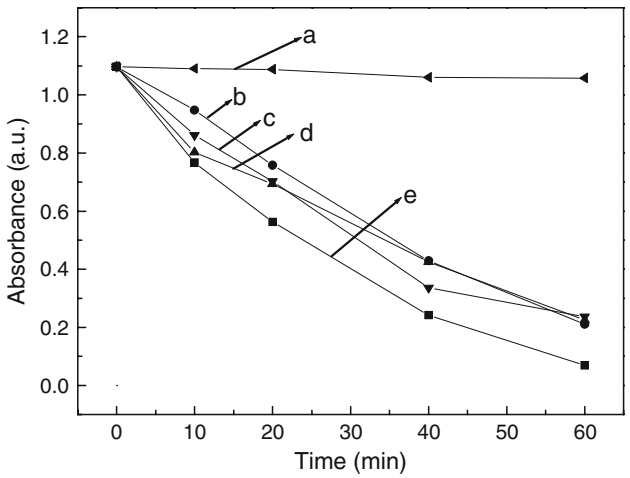

Fig. 8 Plots of absorbance of Rhodamine B (detected at 553 nm) versus time under UV-light irradiation with (a) 0 g TiO_2; (b) 0.02 g TiO_2; (c) 0.02 g TiO_2/H_4TAPP^{6+}; (d) 0.02 g $TiO_2/CoTPPS^{4-}$; (e) 0.02 g TiO_2/porphyrin particles

Table 2 Photoelectrochemical data for three systems

Electrodes	V_{oc} (V)	I_{sc} (mA cm^{-2})	P_{in} (mW cm^{-2})	P_{max} (mW cm^{-2})	FF	η (%)
FTO/TiO_2/$CoTPPS^{4-}$	0.06	0.157	75	2.70×10^{-3}	0.287	3.61×10^{-3}
FTO/TiO_2/H_4TAPP^{6+}	0.10	0.180	75	5.89×10^{-3}	0.327	7.87×10^{-3}
FTO/TiO_2/porphyrin particles	0.21	0.437	75	4.40×10^{-2}	0.479	5.87×10^{-2}

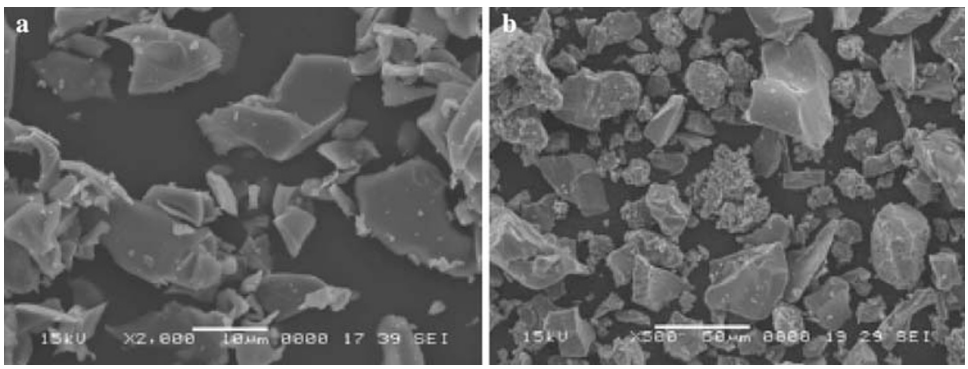

Fig. 7 SEM images of TiO_2 (**a**) and TiO_2/porphyrin particles composite (**b**)

spherical configuration of porphyrin particles contribute to the absorption and transfer of the energy. This type of porphyrin nano- and micro-particles play an important role in the energy conversion. From a practical point of view, it is possible for the porphyrin nano- and micro-particles to have a potential application as photocatalysts used in the semiconductor-assisted photocatalytic reaction to process polluted water caused by the synthetic textile dyes or other commercial colorants during the manufacturing operations. The sensitization mechanism of TiO_2 with porphyrin nano- and micro-particles is complex. Further efforts are underway to investigate the degradation kinetics of Rhodamine B under the same conditions and the influence of the concentration of the porphyrin particles on the photocatalytic behavior of Rhodamine B.

Conclusions

In summary, the nano- and micro-particles constituted by porphyrin H- and J-heteroaggregates are designed and achieved in a simple mixture of two water-soluble porphyrins. The TEM images show that the molar ratios of two porphyrin monomers and the acidity can modulate the morphology and size distribution of the particles. The stability of the particles in different conditions and electrochemical properties are explored. The investigation of photoelectrochemical and photocatalysis activity demonstrates that the porphyrin nano- and micro-particles possess better properties due to their spherical or pyramidal configurations.

References

1. G.M. Whitesides, J.P. Mathias, C.T. Seto, Science **254**, 1312 (1991)
2. J.M. Lehn, Angew. Chem. Int. Ed. Engl. **29**, 1304 (1990)
3. S.C. Doan, S. Shanmugham, D.E. Aston, J.L. McHale, J. Am. Chem. Soc. **127**, 5885 (2005)
4. T. Hatano, M. Takeuchi, A. Ikeda, S. Shinkai, Org. Lett. **5**, 1395 (2003)
5. J.H. Fuhrhop, U. Bindig, U. Siggel, J. Am. Chem. Soc. **115**, 11036 (1993)
6. N. Micali, A. Romeo, R. Lauceri, R. Purrello, F. Mallamace, L.M. Scolaro, J. Phys. Chem. B **104**, 9416 (2000)
7. N.C. Maiti, S. Mazumdar, N. Periasamy, Curr. Sci. **70**, 997 (1996)
8. N.C. Maiti, S. Mazumdar, N. Periasamy, J. Phys. Chem. B **102**, 1528 (1998)
9. E.B. Fleischer, J.M. Palmer, T.S. Srivastava, A. Chatterjee, J. Am. Chem. Soc. **93**, 3162 (1971)
10. F. Mallamace, N. Micali, S. Trusso, L.M. Monsù Scolaro, A. Romeo, A. Terracina, R.F. Pasternack, Phys. Rev. Lett. **76**, 4741 (1996)
11. R. Rotomskis, R. Augulis, V. Snitka, R. Valiokas, B. Liedberg, J. Phys. Chem. B **108**, 2833 (2004)
12. L.A. Lucia, T. Yui, R. Sasai, S. Takagi, K. Takagi, H. Yoshida, D.G. Whitten, H. Inoue, J. Phys. Chem. B **107**, 3789 (2003)
13. M.D. Ward, Chem. Soc. Rev. **26**, 365 (1997)
14. B. O'Regan, J. Moser, M. Anderson, M. Grätzel, J. Phys. Chem. **94**, 8720 (1990)
15. S. Cherian, C.C. Wamser, J. Phys. Chem. B **104**, 3624 (2000)
16. B. O'Regan, M. Grätzel, Nature **353**, 737 (1991)
17. T.M.R. Viseu, G. Hungerford, M.I.C. Ferreira, J. Phys. Chem. B **106**, 1853 (2002)
18. D.M. Guldi, I. Zilbermann, G.A. Anderson, K. Kordatos, M. Prato, R. Tafuro, L. Valli, J. Mater. Chem. **14**, 303 (2004)
19. P.V. Kamat, S. Barazzouk, K.G. Thomas, S. Hotchandani, J. Phys. Chem. B **104**, 4014 (2000)
20. P.V. Kamat, S. Barazzouk, S. Hotchandani, K.G. Thomas, Chem. Eur. J. **6**, 3914 (2000)
21. P.K. Sudeep, B.I. Ipe, K.G. Thomas, M.V. George, S. Barazzouk, S. Hotchandani, P.V. Kamat, Nano. Lett. **2**, 29 (2002)
22. S. Park, E. DiMasi, Y.-Il. Kim, W.Q. Han, P.M. Woodward, T. Vogt, Thin Solid Films **515**, 1250 (2006)
23. T. Sreethawong, Y. Suzuki, S. Yoshikawa, J. Solid State Chem. **178**, 329 (2005)
24. J. Arana, J.M. Dona-Rodriguez, O. Gonzalez-Diaz, E. Tello Rendon, J.A. Herrera Melian, G. Colon, J.A. Navio, J. Pena Perez, J. Mol. Catal. A: Chem. **215**, 153 (2004)
25. R. Suarez-Parra, I. Hernandez-Perez, M.E. Rincon, S. Lopez-Ayala, M.C. Roldan-Ahumada, Sol. Energy Mater. Sol. Cells **76**, 189 (2003)
26. X.Q. Li, L.E. Zhang, J. Mu, Colloids Surf. A: Physicochem. Eng. Asp. **311**, 187 (2007)
27. N. Micali, F. Mallamace, A. Romeo, R. Purrello, L. Monsù Scolaro, J. Phys. Chem. B **104**, 5897 (2000)
28. Z. Ou, H. Yao, K. Kimura, Chem. Lett. **35**, 782 (2006)
29. A.D. Adler, F.R. Longo, F. Kampas, J. Kim, J. Inorg. Nucl. Chem. **32**, 2443 (1970)
30. N.A. Kotov, F.C. Meldrum, J.H. Fendler, J. Phys. Chem. **98**, 8827 (1994)
31. V. Subramanian, E. Wolf, P.V. Kamat, J. Phys. Chem. B **105**, 11439 (2001)
32. K. Pavel, L. Kamil, Z. Zdeněk, J. Mol. Liq. **131**, 200 (2007)
33. B.W. van der Meer, *Resonance Energy Transfer: Theory and Data* (VCH, New York, 1994)
34. M. Kasha, *Physical and Chemical Mechanisms in Molecular Radiation Biology* (Plenum Press, New York, 1991)
35. P. Gregory Van Patten, A.P. Shreve, R.J. Donohoe, J. Phys. Chem. B **104**, 5986 (2000)
36. Z.M. Ou, H. Yao, K. Kimura, J. Photochem. Photobiol. A: Chem. **189**, 7 (2007)
37. I. Gupta, M. Ravikanth, J. Photochem. Photobiol. A: Chem. **177**, 156 (2006)
38. J.H. Ha, S. Ko, C.H. Lee, W.Y. Lee, Y.R. Kim, Chem. Phys. Lett. **349**, 271 (2001)
39. A. Fuerte, A. Corma, M. Iglesias, E. Morales, F. Sánchez, Catal. Lett. **101**, 99 (2005)
40. T. Ye, Y. He, E. Borguet, J. Phys. Chem. B **110**, 6141 (2006)
41. K.S. Suslick, S.B. Choe, A.A. Cichowlas, M.W. Grinstaff, Nature **353**, 414 (1991)
42. A. Hagfeldt, M. Grätzel, Acc. Chem. Res. **33**, 26 (2000)